

Role of the nano amorphous interface in the crystallization of Sb_2Te_3 towards non-volatile phase change memory: insights from first principles†

Cite this: *Phys. Chem. Chem. Phys.*, 2014, 16, 10810

Xue-Peng Wang,^a Nian-Ke Chen,^a Xian-Bin Li,^{*a} Yan Cheng,^b X. Q. Liu,^c Meng-Jiao Xia,^b Z. T. Song,^b X. D. Han,^c S. B. Zhang^{*ad} and Hong-Bo Sun^{*a}

The nano amorphous interface is important as it controls the phase transition for data storage. Yet, atomic scale insights into such kinds of systems are still rare. By first-principles calculations, we obtain the atomic interface between amorphous Si and amorphous Sb_2Te_3 , which prevails in the series of Si–Sb–Te phase change materials. This interface model reproduces the experiment-consistent phenomena, *i.e.* the amorphous stability of Sb_2Te_3 , which defines the data retention in phase change memory, and is greatly enhanced by the nano interface. More importantly, this method offers a direct platform to explore the intrinsic mechanism to understand the material function: (1) by steric effects through the atomic “channel” of the amorphous interface, the arrangement of the Te network is significantly distorted and is separated from the p-orbital bond angle in the conventional phase-change material; and (2) through the electronic “channel” of the amorphous interface, high localized electrons in the form of a lone pair are “projected” to Sb_2Te_3 from amorphous Si by a proximity effect. These factors set an effective barrier for crystallization and improve the amorphous stability, and thus data retention. The present research and scheme sheds new light on the engineering and manipulation of other key amorphous interfaces, such as $\text{Si}_3\text{N}_4/\text{Ge}_2\text{Sb}_2\text{Te}_5$ and $\text{C}/\text{Sb}_2\text{Te}_3$, through first-principles calculations towards non-volatile phase change memory.

Received 28th December 2013,
Accepted 4th March 2014

DOI: 10.1039/c3cp55476g

www.rsc.org/pccp

Introduction

Compared to conventional dynamic random access memory (DRAM), phase change memory (PCM) is non-volatile as the data bit can be stored when the electric power is off.^{1,2} As such, data retention is a critical performance criterion in PCM. Generally, the working mechanism depends mainly on the kind of phase change material, such as chalcogenides.³ Such a material can undergo fast and reversible transitions between the amorphous and crystalline phases, whilst a significant

electrical/optical contrast still exists.^{4–7} Compared to the most popular Ge–Sb–Te alloys,⁸ Si–Sb–Te materials have recently been demonstrated to hold high data retention for PCM; the 10-year retention temperature of amorphous $\text{Si}_3\text{Sb}_2\text{Te}_3$ has been reported to be 393 K, in contrast to 347 K for $\text{Ge}_2\text{Sb}_2\text{Te}_5$,⁹ which exhibits promise for high temperature applications based on this PCM material. Therefore, gaining insight into the Si–Sb–Te material network, as well as its function in the phase transition, is a key step to further explore high retention PCM.

$\text{Si}_x\text{Sb}_2\text{Te}_3$, where $3 < x < 3.5$, has been proven to be the optimal composition for Si–Sb–Te materials. Thus, this composition can be regarded as Si-alloyed Sb_2Te_3 . Previous TEM experiments have shown that phase separation usually occurs in Si–Sb–Te alloys,^{10,11} *i.e.* amorphous Si (a-Si) and amorphous Sb_2Te_3 (a-ST) are wrapped around each other in the form of a reticular structure. In other words, a special characteristic of Si–Sb–Te is that there are a lot of nano amorphous interfaces knitted into the material network. In fact, it is hard to stabilize the amorphous phase of Sb_2Te_3 alone, and it has poor data retention, whilst Si implantation significantly increases the stability of the amorphous phase.¹² Generally, materials near the interface or surface should have different functions from

^a State Key Laboratory on Integrated Optoelectronics, College of Electronic Science and Engineering, Jilin University, Changchun, China.

E-mail: lixianbin@jlu.edu.cn, hbsun@jlu.edu.cn

^b State Key Laboratory of Functional Materials for Informatics and Nanotechnology Laboratory, Shanghai Institute of Micro-System and Information Technology, Chinese Academy of Sciences, Shanghai, China

^c Institute of Microstructure and Property of Advanced Materials, Beijing University of Technology, Beijing, China

^d Department of Physics, Applied Physics & Astronomy, Rensselaer Polytechnic Institute, Troy, New York, USA. E-mail: zhangs9@rpi.edu

† Electronic supplementary information (ESI) available. See DOI: 10.1039/c3cp55476g

those in the bulk of the material.^{13,14} Thus, an important question is naturally raised here: what is the role of this nano amorphous interface in Si-Sb-Te, and how does the amorphous Si affect the phase transition of Sb₂Te₃ through such an interface during data storage?

Atomic scale simulation is a powerful tool used to comprehend material behaviors and their rules for use in practical applications. In particular, *ab initio* molecular dynamics (AIMD) has been employed to explore the microscopic origin of ultrafast data storage in many PCM materials, which has been very successful. For example, Sun *et al.* in 2007¹⁵ studied the phase change dynamics in a Ge-Sb-Te system, and suggested a melting behavior where the amorphization is a result of the formation of linear and tangled clusters in the (111) plane, whilst order was kept in the perpendicular [111] direction. In 2008, Elliott *et al.*¹⁶ showed how connected square ring structures of the rocksalt phase are formed during the cooling of a melt, and how they are subsequently quenched in the amorphous phase. In 2011, Li *et al.*¹⁷ proposed excitation-induced direct amorphization without melting to achieve data storage. However, to our best knowledge, few reports concentrate on the atomic interface model between two amorphous phases, like that between a-Si and a-ST in Si-Sb-Te. Therefore, there is urgent demand for a careful investigation on such a nano interface system for PCM, to target better non-volatile performance.

In this work, we obtain the structure of the atomic interface between a-Si and a-ST by AIMD. Important insight into why a-Si enhances the stability of a-ST through the nano interface is illustrated. Both bond geometry and electronic structure analyses demonstrate that the local environment of Te in Sb₂Te₃ has been evidently modulated with a-Si through their interfaces. Generally, the Te framework defines the long-range order in Te-based PCM materials. Consequently, the original bonding which is similar between the amorphous and crystalline phases of Te in bulk Sb₂Te₃ can be clearly separated near the interface. As a proximity effect from the disorder in a-Si, this interface with a-ST exhibits significantly highly localized electrons in the form of a lone pair. Therefore, despite the atomic local motifs or electronic states, the nano interface greatly enhances the stability of a-ST and thus, the device retention.

Methods

The present study employs density functional theory,^{18,19} as implemented in the Vienna *Ab initio* Simulation Package (VASP) code.²⁰ The electron-ion interaction is described by the projector augmented wave (PAW) pseudopotential,²¹ and the electronic exchange-correlation interaction is described by the generalized gradient approximation (GGA)²² using the Perdew-Wang 1991 (PW91)²³ functional. In the AIMD simulations, we use the *NVT* canonical ensemble (where the number of atoms, the volume, and the temperature are constant in the ensemble), in which the Nosé-Hoover thermostat is used to control the temperature.^{24,25} Our model is built on the basis of a Sb₂Te₃ hexagonal unit cell; a 4 × 2 × 1 supercell is employed, then half of the atoms are

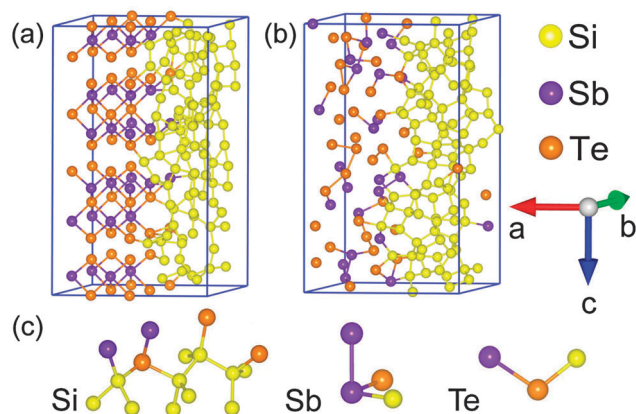


Fig. 1 (a) Initial interface structure model of Si and Sb₂Te₃ for the AIMD simulation. (b) Final amorphous interface model obtained by AIMD melt-quenching method. (c) Representative local motifs centering at Si, Sb and Te at the connection of the interface. Color coding: yellow for Si, purple for Sb, and orange for Te.

deleted and filled by Si atoms according to the experimental a-Si density,²⁶ see Fig. 1(a). As a result, the model contains 156 atoms (including 96 Si, 24 Sb, and 36 Te), and the interface is built parallel to the *c* axis (and also parallel to the *b*-*o*-*c* plane, here labelled *a*, *b*, *c* for the cell-size direction in Fig. 1) of the initial Sb₂Te₃ supercell. Internal atomic relaxation is carried out to correct the local structure after random Si filling before AIMD. The AIMD for the interface calculations employs an energy cutoff of 270 eV, *K*-point set of 2 × 2 × 1, Gaussian smearing with 0.1 eV, and no spin.

The interface structure between a-Si and a-ST is built using the AIMD melt-quenching technique. To reproduce the experimentally-observed phase separation^{10,11} during the AIMD simulation, the Sb₂Te₃ part of the supercell was locked, and the rest of the Si was melted at 3000 K, then quenched to 1900 K, a little higher than its melting point (*T*_m of Si, ~1700 K),²⁷ and finally quenched to 300 K. This (Si amorphization) is the first step to build the amorphous interface. In the second step, the a-Si was locked, and the amorphization of Sb₂Te₃ was carried out by melting at 3000 K, then quenching at 1000 K (*T*_m of Sb₂Te₃, ~900 K),²⁸ and finally quenching at 300 K. All of the above AIMDs run for 6 ps. In the third step, the two free amorphous parts were annealed together at 300 K for 9 ps to correct the error induced by the locking procedure and obtain the final amorphous interface (i-ST) in Fig. 1(b). To compare the material function, a bulk Sb₂Te₃ model (b-ST) without an interface effect was also amorphized using the same method as above. The supercell parameters and models for i-ST, b-ST, and bulk Si (b-Si) are listed in Part I of the ESI.†

Result and discussion

To evaluate the reliability of the theoretical interface model, two crystallization AIMDs were run at 600 K in both of the i-ST and b-ST models for 36 ps. Fig. 2(a) displays their initial and final states during the crystallization. Immediately, a clear

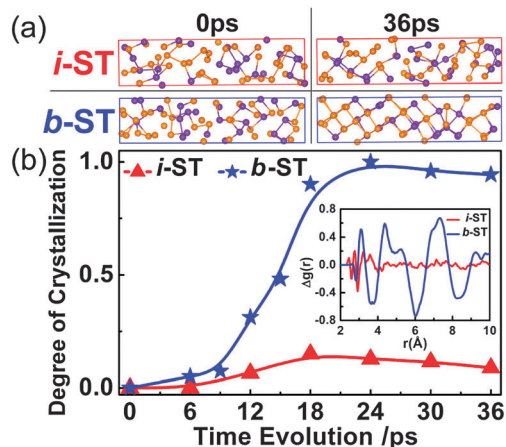


Fig. 2 Crystallization states for i-ST and b-ST. (a) Structure comparison between the initial and final steps of the crystallization. (b) Degree of crystallization during the whole process in order to see the crystallization dynamics. Inset shows the change in the pair correlation function (PCF) between the initial and final steps. The color coding of the elements is the same as in Fig. 1.

change from disorder to order indicates that b-ST has been successfully crystallized. In stark contrast, i-ST retains a mostly amorphous state even after the whole annealing. To quantify this, we compared the pair correlation function (PCF, $g(r,t)$) for the two models, since the function can be indexed as the degree of long-range order of the atomic arrangement. In the inset of Fig. 2(b), we compare the $\Delta g(r) = g(r,36ps) - g(r,0ps)$. Once again, b-ST showed significant variation in the middle and long ranges ($>4 \text{ \AA}$), while the $\Delta g(r)$ of i-ST was almost preserved at zero. In order to watch the material respond dynamically to the annealing, a “degree of crystallization” was defined (see Part III in ESI† for the details), and the result is shown in Fig. 2(b). For b-ST, the crystallization process suddenly accelerates at 12 ps, and is essentially complete after 24 ps, after which the “degree” remains constant. However, for i-ST, the degree of crystallization is less than 15% during the whole 36 ps simulation, indicating no obvious changes in its disorder. Thus, not only the crystallization degree, but also the speed of crystallization in Sb_2Te_3 is significantly suppressed in the presence of the interface. These results are consistent with the phenomenon observed experimentally in Si-Sb-Te:^{10,29} with an interface between a-Si and a-ST, crystallization of $\text{Si}_x\text{Sb}_2\text{Te}_3$ becomes more difficult and slower, thereby enhancing the stability of amorphous Sb_2Te_3 (this is also supported by the free energy analysis in Part IV of the ESI†). In other words, using the present method to create an amorphous interface model is quite reasonable.

On the basis of such a reliable model, it is possible to carry out careful analyses to explore the underlying phase-transition mechanism in i-ST. Firstly, the atomic local environments are observed by analysing the distribution of the coordination number (CN) and the bond angle distribution (BAD). The BAD and CN are closely related to the distance “cutoff”; if the distance between two atoms is shorter than the cutoff, these two atoms are regarded as bonding. Our cutoffs are selected

Table 1 Cutoff distances of element pairs for structural analysis

	Si-Si (Å)	Si-Sb (Å)	Si-Te (Å)	Sb-Sb (Å)	Sb-Te (Å)	Te-Te (Å)
i-ST	2.761	2.918	2.918	3.035	3.230	3.074
b-ST & b-Si	2.800	—	—	3.152	3.191	3.113

according to the first valley of their partial PCFs, and summarized in Table 1. Fig. 3 compares the results between amorphous b-ST and i-ST. For b-ST, both the Sb and Te atoms have a BAD symmetrically centering at around 90° , which is the signature for p-orbital bonding in a conventional PCM material.³⁰ For i-ST, Sb keeps the 90° -centered BAD, which is consistent with the typical Sb local motif at the interface shown in Fig. 1(c). However, in contrast, the interface has a significant impact on the BAD of Te, which has an extra distribution from 100° to 130° . In other words, the local environment of Te (see its typical motif in Fig. 1(c)) has been disturbed to a certain degree in the presence of the interface, and deviates from the original p-orbital bonding characteristic. In the CN comparison, the interface model does not evidently change from the bulk model (see the insets of Fig. 3), *i.e.* the CN of Sb and Te are still mainly located at 3 and 2 in i-ST, respectively. Fig. S4 in Part V of the ESI† shows that Si displays almost no variation in the BAD and CN between the interface and bulk models. The CN of 4 and the BAD of around 109° indicate that the robust sp^3 bonding characteristic always exists in a-Si, as shown in Fig. 1(c). Therefore, in the amorphous interface model, all of the elements still obey the 8- N coordination rule, however, strong disorder in the a-Si network obviously distorts the local environment of Te in Sb_2Te_3 , due to the steric effect from the interface connection.

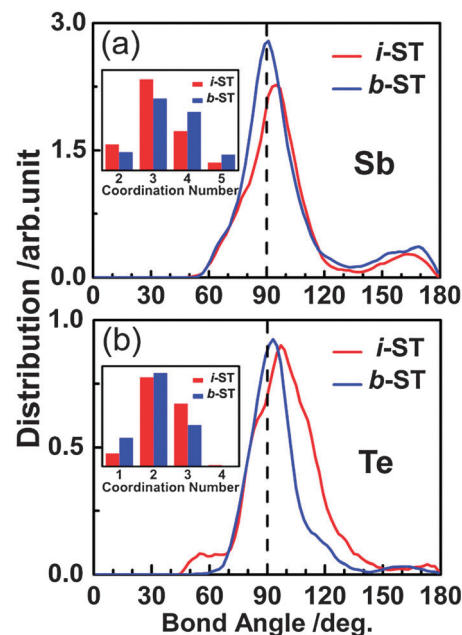


Fig. 3 The bond angle distributions (BADs) of Sb and Te, compared between the amorphous i-ST and b-ST. The black dashed line highlights the p-orbital bond angle of 90° for reference. The insets show the corresponding coordination number (CN) distributions.

To quantify the local motif of the material, for example a tetrahedron or octahedron environment, the local order parameter (LOP, q) is sensitive and useful:^{31,32}

$$q = 1 - \frac{3}{8} \sum_{i>k} \left(\frac{1}{3} + \cos \theta_{ijk} \right)^2,$$

where the sum is calculated for the couples of atoms bonded to the central atom j . The distributions of the LOP q for the Si, Sb and Te atoms for different coordination numbers are summarized in Fig. 4. The standard q values for the 6-fold octahedral (all atoms have the 90° bond angle), 5-fold octahedral, 4-fold octahedral and 3-fold octahedral motifs are 0, 0.333, 0.625 and 0.875, respectively, whereas the standard value for a 4-fold tetrahedral motif is just 1. (1) In the presence of the interface, the q of Si at a CN of 4 is close to 1, indicating that the original sp^3 -hybrid bonding characteristic has been enhanced as shown in Fig. 4(a) and (a*). (2) In the presence of the interface, all of

the Sb atoms have a tendency to get together to form the 3-fold octahedral local motif, which also indicates an enhancement of the original p-orbital bonding in Fig. 4(b) and (b*). (3) However, in Fig. 4(c) and (c*), Te shows a very unusual variation in the presence of the interface. For the CN of 3, the almost standard 3-fold octahedral motif in b-ST has been strongly disturbed and the q centering at 0.875 differs from the broad range of 0.6–0.9 observed in i-ST. For the CN of 2, it is more suitable to use the BAD rather than the LOP to observe the variation. Once again, an obvious separation from 90° occurs in the inset of Fig. 4(c*). All of these observations illustrate that Te suffers from the presence of the amorphous interface, which destroys its original local order characteristic, *i.e.* the p-orbital octahedral motif in i-ST.

To reveal the bonding characteristics and intrinsic electronic distribution of Sb_2Te_3 controlled by the interface, it is necessary to carry out electronic structure analyses. First, Bader analysis,³³ which indicates the charge transfer between atoms, was carried out. As a comparison, we also calculated this for the amorphous bulk Si and Sb_2Te_3 without an interface. Table 2 shows the results compared to the number of atomic valence electrons. At a glance, it seems that electrons transfer from Si to Sb and Te, compared to the bulk phases. In fact, in b-ST, Te also gains electrons from Sb due to their electronegativities.³⁴ Linking this to the structure analysis above, it can be deduced that Si donates extra electrons to Te in i-ST. This external charge transfer lessens the original “Sb to Te” bonding donation, which decreases the CN of Sb, as shown before in the presence of the interface.

To identify the electronic characteristics in the space, Fig. 5 shows the electron localization function (ELF)³⁵ distribution in amorphous i-ST and b-ST. We selected a relatively large value of 0.92 to display the highly localized electrons. It is very clear to see that Si places such highly localized electrons in the center of the covalent bonds. In contrast, the highly localized electrons in Sb_2Te_3 are not distributed at the bond center, but are in the form of lone-pair electrons. We can see significantly different amounts of these lone-pair electrons between i-ST and b-ST. In fact, we also chose other high ELF values for comparison, see Part VI of the ESI.† All of these show that the number of highly localized electrons is larger through the amorphous interface in i-ST than that in b-ST. This shows that the high electron localization characteristic in amorphous Si has “infected” that of Sb_2Te_3 . Considering the charge transfer from Si to Sb_2Te_3 by Bader analysis as above, lone-pair electrons which have the standard form of an s^2 pair in Sb or s^2-p^2 pairs in Te would be enhanced. On the other hand, for Sb (s^2p^3), the increment in

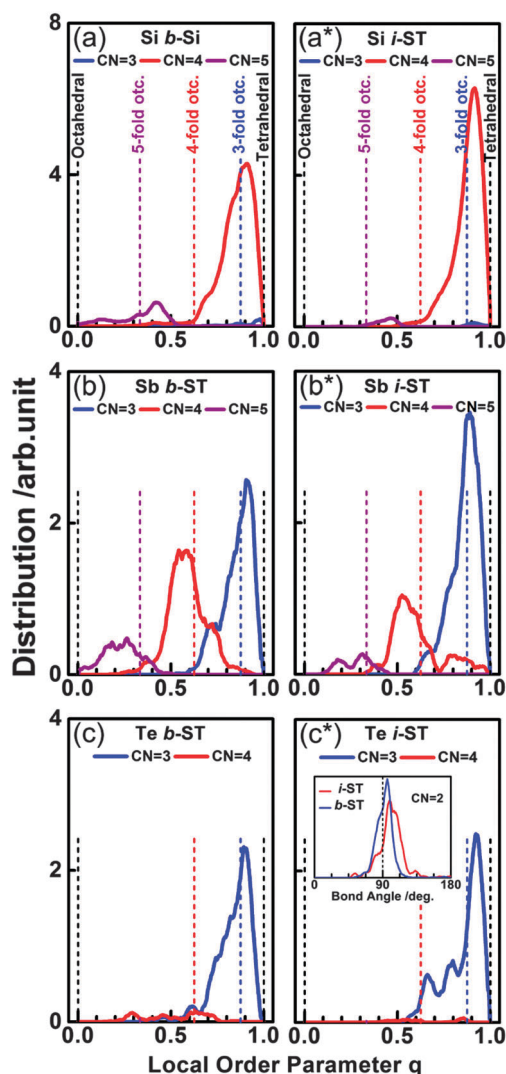


Fig. 4 Local order parameters (LOPs) in the i-ST and b-ST models for the three elements: Si (a)–(a*), Sb (b)–(b*), and Te (c)–(c*). Inset in (c*) shows the BAD of Te with a CN of 2.

Table 2 Results of the Bader charge analysis of the interface structure, bulk amorphous Si and bulk amorphous Sb_2Te_3 . The valence electron of the atom state is referenced

	Si	Sb	Te
Interface	3.955	4.806	6.251
Bulk Si & Sb_2Te_3	4	4.689	6.207
Atom	4	5	6

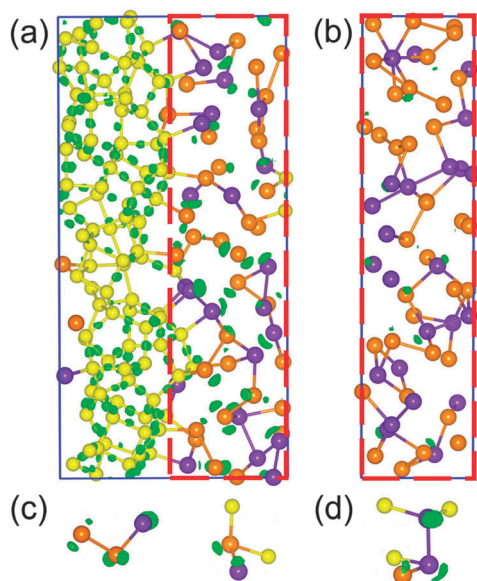


Fig. 5 Distribution of the highly localized electrons in (a) i-ST and (b) b-ST with an isosurface of 0.92 in the electron localization function (ELF). Representative local motifs with a lone pair around (c) Te and (d) Sb. The color coding of the elements is the same as in Fig. 1.

the number of the CN of 3 in i-ST supports its electronic configuration, which has three normal p-orbital bonds plus a lone s^2 pair, as shown in Fig. 5(d): a single ELF “cap” around a typical “purple” Sb atom. For Te (s^2p^4), two typical motifs are shown, for the CN of 2, with two “caps”, and the CN of 3, with a single “cap”. It can be understood that 2-CN Te with two bonds favors s^2 plus p^2 lone pairs, while 3-CN Te with three bonds favors just the s^2 lone pair. The significant variation in the Te bond angle from $\sim 90^\circ$ in b-ST, to $\sim 110^\circ$ in i-ST (off the octahedral motif, see Fig. 5(c)), could be possibly explained by the enhanced hybridization of the s^2 and p^2 lone pairs in the 2-CN motifs, similar to that in a H_2O molecule. Therefore, the octahedron-favored resonant bonding³⁶ is naturally suppressed by the presence of the nano interface, which can act as a very effective barrier in crystallization, and thus stabilize the amorphous data bit.

In fact, we also checked the model effect from a different interface orientation. When the interface is vertical to the c axis, the stability of amorphous Sb_2Te_3 would be weakened (see details in Part VII of the ESI[†]). This could possibly be explained by the inherent five-layer structural unit of Sb_2Te_3 , with a relatively isolated electronic configuration, being just vertical to the c axis. Thus, the interface vertical to the c axis may have less impact on the Sb_2Te_3 bonding environment. We conclude that the present interface model (parallel to c axis) has a more significant role in stabilizing amorphous Sb_2Te_3 .

Conclusion

A Si/ Sb_2Te_3 nano amorphous interface, of importance for PCM, has been established on an atomic scale using a first-principles molecular dynamics simulation. Systematic analyses of the

bond geometry and electronic structure reveal that the framework of the Te element in Sb_2Te_3 is significantly distorted and separated from the octahedral local environment by the nano interface. With electronic donation from a-Si through the interface, more localized electrons can be found in the form of a lone pair in Sb_2Te_3 . Such discrepancy from the normal p-orbital bonding in the prevailing PCM materials provides a very effective barrier to stabilize the amorphous Sb_2Te_3 data bit. The crystallization simulations for i-ST and b-ST together further support the conclusions made above. Therefore, this shows the inherent mechanism of Si to improve Sb_2Te_3 stability in Si–Sb–Te PCM materials. To our knowledge, this may be the first attempt to make an effort to build an atomic interface between two amorphous phases for PCM applications. In fact, the amorphous nano interface structure is popular in PCM materials and devices, such as a-ST/a-C, a-GST/a-Si₃N₄. The present study can be extended to such systems in order to explore their intrinsic physics for PCM applications.

Acknowledgements

This work was supported by the NSFC (No. 11104109, 11374119), China Postdoctoral Science Foundation (No. 2013T60315), and 973 Program (No. 2014CB921303). SBZ is supported by the U.S. DOE Office of Basic Energy Sciences (No. DE-SC0002623). The high performance computing center (HPCC) of Jilin University was also acknowledged for the calculation resource.

Notes and references

- 1 M. Wuttig and N. Yamada, *Nat. Mater.*, 2007, **6**, 824.
- 2 D. Lencer, M. Salinga, B. Grabowski, T. Hickel, J. Neugebauer and M. Wuttig, *Nat. Mater.*, 2008, **7**, 972.
- 3 S. R. Ovshinsky, *Phys. Rev. Lett.*, 1968, **21**, 1450.
- 4 D. Lencer, M. Salinga and M. Wuttig, *Adv. Mater.*, 2011, **23**, 2030.
- 5 M. A. Caldwell, R. Jeyasingh, H.-S. Philip Wong and D. J. Milliron, *Nanoscale*, 2012, **4**, 4382.
- 6 A. L. Lacaita and D. J. Wouters, *Phys. Status Solidi A*, 2008, **205**, 2281.
- 7 A. V. Kolobov, P. Fons, A. I. Frenkel, A. L. Ankudinov, J. Tominaga and T. Uruga, *Nat. Mater.*, 2004, **3**, 703.
- 8 N. Yamada, E. Ohno, K. Nishiuchi, N. Akahira and M. Takao, *J. Appl. Phys.*, 1991, **69**, 2849.
- 9 J. Feng, Z. F. Zhang, Y. Zhang, B. C. Cai and Y. Y. Lin, *J. Appl. Phys.*, 2007, **101**, 074502.
- 10 F. Rao, Z. T. Song, K. Ren, X. L. Zhou, Y. Cheng, L. C. Wu and B. Liu, *Nanotechnology*, 2011, **22**, 145702.
- 11 Y. Cheng, N. Yan, X. D. Han, Z. Zhang, T. Zhang, Z. T. Song, B. Liu and S. L. Feng, *J. Non-Cryst. Solids*, 2010, **356**, 884.
- 12 Z. H. Zhang, S. N. Song, Z. T. Song, Y. Cheng, Y. F. Gu and B. Chen, *Appl. Phys. Lett.*, 2013, **102**, 252106.
- 13 L. Martin, G. Vallverdu, H. Martinez, F. Le Cras and I. Baraille, *J. Mater. Chem.*, 2012, **22**, 22063.

- 14 L. L. Huang, X. Z. Chen, B. F. Bai, Q. F. Tan, G. F. Jin, T. Zentgraf and S. Zhang, *Light: Sci. Appl.*, 2013, **2**, e70.
- 15 Z. M. Sun, J. Zhou and R. Ahuja, *Phys. Rev. Lett.*, 2007, **98**, 055505.
- 16 J. Hegedüs and S. R. Elliott, *Nat. Mater.*, 2008, **7**, 399.
- 17 X. B. Li, X. Q. Liu, X. Liu, D. Han, Z. Zhang, X. D. Han, H. B. Sun and S. B. Zhang, *Phys. Rev. Lett.*, 2011, **107**, 015501.
- 18 P. Hohenberg and W. Kohn, *Phys. Rev.*, 1964, **136**, B864.
- 19 W. Kohn and L. J. Sham, *Phys. Rev.*, 1965, **140**, A1133.
- 20 G. Kresse and J. Furthmüller, *Phys. Rev. B: Condens. Matter Mater. Phys.*, 1996, **54**, 11169.
- 21 P. E. Blöchl, *Phys. Rev. B: Condens. Matter Mater. Phys.*, 1994, **50**, 17953.
- 22 J. P. Perdew and Y. Wang, *Phys. Rev. B: Condens. Matter Mater. Phys.*, 1986, **33**, 8800.
- 23 J. P. Perdew, J. A. Chevary, S. H. Vosko, K. A. Jackson, M. R. Pederson, D. J. Singh and C. Fiolhais, *Phys. Rev. B: Condens. Matter Mater. Phys.*, 1992, **46**, 6671.
- 24 S. Nosé, *Prog. Theor. Phys. Suppl.*, 1991, **103**, 1.
- 25 S. Y. Xie, X. B. Li, Y. Y. Sun, Y. L. Zhang, D. Han, W. Q. Tian, W. Q. Wang, Y. S. Zheng, S. B. Zhang and H. B. Sun, *Carbon*, 2013, **52**, 122.
- 26 J. S. Custer, M. O. Thompson, D. C. Jacobson, J. M. Poate, S. Roorda, W. C. Sinke and F. Spaepen, *Appl. Phys. Lett.*, 1994, **64**, 437.
- 27 E. P. Donovan, F. Spaepen, D. Turnbull, J. M. Poate and D. C. Jacobson, *Appl. Phys. Lett.*, 1983, **42**, 698.
- 28 Y. Zhang, J. Feng, Z. F. Zhang, B. C. Cai, Y. Y. Lin and T. A. Tang, *Appl. Surf. Sci.*, 2008, **254**, 56028.
- 29 X. L. Li, F. Rao, Z. T. Song, K. Ren, W. L. Liu and Z. M. Sun, *Appl. Surf. Sci.*, 2011, **257**, 4566.
- 30 S. Caravati, M. Bernasconi and M. Parrinello, *Phys. Rev. B: Condens. Matter Mater. Phys.*, 2010, **81**, 014201.
- 31 S. Caravati, M. Bernasconi, T. D. Kuhne, M. Krack and M. Parrinello, *Appl. Phys. Lett.*, 2007, **91**, 171906.
- 32 J. R. Errington and P. G. Debenedetti, *Nature*, 2001, **409**, 318.
- 33 G. Henkelman, A. Arnaldsson and H. Jónsson, *Comput. Mater. Sci.*, 2006, **36**, 354.
- 34 W. Gordy and W. J. Orville Thomas, *J. Chem. Phys.*, 1956, **24**, 439.
- 35 A. Savin, O. Jepsen, J. Flad, O. K. Andersen, H. Preuss and H. G. von Schnering, *Angew. Chem., Int. Ed. Engl.*, 1992, **30**, 187.
- 36 K. Shportko, S. Kremers, M. Woda, D. Lencer, J. Roberson and M. Wuttig, *Nat. Mater.*, 2008, **7**, 653.